

Article

# Effect of $\text{Fe}_2\text{O}_3$ – $\text{ZrO}_2$ Catalyst Morphology on Sulfamethazine Degradation in the Fenton-Like Reaction

Pan Gao \* , Mengjie Hao , Yue He, Yuan Song and Shaoxia Yang \*

National Engineering Laboratory for Biomass Power Generation Equipment, North China Electric Power University, Beijing 102206, China; haomengjie2018@163.com (M.H.); heyue61@163.com (Y.H.); songyuan\_0601@163.com (Y.S.)

\* Correspondence: gaopan@ncepu.edu.cn (P.G.); yangshaoxia@ncepu.edu.cn (S.Y.); Tel.: +86-106-177-2456 (S.Y.)

Received: 17 December 2018; Accepted: 9 January 2019; Published: 14 January 2019



**Abstract:**  $\text{Fe}_2\text{O}_3$ – $\text{ZrO}_2$  catalysts with different morphologies (nanoplates (HZNPs), nanorods (HZNRs), nanocubes (HZNCs), and nanotubes (HZNTs)) were prepared by a hydrothermal method to investigate the effect of the morphology on the catalytic performance in the Fenton-like reaction for sulfamethazine (SMT) degradation. The  $\text{Fe}_2\text{O}_3$ – $\text{ZrO}_2$  catalysts were characterized by scanning electron microscope (SEM), X-ray diffraction (XRD), X-ray photoelectron spectroscopy (XPS), and Brunauer–Emmett–Teller (BET) analysis. The  $\text{H}_2\text{O}_2$  adsorption and the  $\text{Fe}^{2+}$  density sites on the  $\text{Fe}_2\text{O}_3$ – $\text{ZrO}_2$  catalysts had a close relationship with the morphologies and exhibited an important effect on the ·OH formation in the Fenton-like reaction. Free ·OH radicals were the main oxidative species in the reaction, and the normalized ·OH concentration per surface area of the catalysts was 4.52, 2.24, 2.20, and 0.37  $\mu\text{mol}/\text{m}^2$  for HZNPs, HZNRs, HZNCs, and HZNTs, respectively. The  $\text{Fe}_2\text{O}_3$ – $\text{ZrO}_2$  catalysts with different morphologies showed good catalytic performance, and the order of SMT degradation was HZNPs > HZNRs > HZNCs > HZNTs. Total SMT removal was achieved in the Fenton-like reaction over HZNPs at pH 3.0 and 45 °C after 240 min.

**Keywords:** Fenton-like reaction; hematite; structure-dependent reactivity;  $\text{ZrO}_2$ ; sulfamethazine

## 1. Introduction

Advanced oxidation processes (AOPs), involving ozone, photocatalysis, electrochemical oxidation, Fenton reaction and wet air oxidation and so on, are efficient treatment technologies for degrading toxic and/or refractory organic compounds [1–4]. Among the AOPs, the Fenton reaction ( $\text{Fe}^{2+}/\text{H}_2\text{O}_2$ ), as a green, simple and efficient process, can remove bio-refractory organic compounds. However, the application of the traditional Fenton reaction is limited in wastewater treatment, due to a narrow pH range and sludge production [2]. The heterogeneous Fenton-like process can avoid these shortcomings to some extent. Iron-based oxides (such as  $\text{Fe}_3\text{O}_4$ ,  $\text{Fe}_2\text{O}_3$ ,  $\text{FeOOH}$ ,  $\text{Fe}^0$ , etc.), which are environmental-friendly and easily available materials, exhibit good performance in the heterogeneous Fenton-like reaction [3–8]. Compared to  $\text{Fe}_3\text{O}_4$ , hematite ( $\alpha\text{-Fe}_2\text{O}_3$ ) showed good chemical stability along with poor activity. The development of iron oxide catalysts with good activity and stability is a crucial challenge for the heterogeneous Fenton-like reaction.

The performance of heterogeneous catalysts not only depends on their chemical composition, size, and surface area but also on the morphology and arrangement manner of the surface atoms. Hematite with different morphologies (such as nanocubes, nanorods, nanobelts, nanoflowers, etc.) has been widely focused [9,10]. The literature shows that the morphology of  $\alpha\text{-Fe}_2\text{O}_3$  can affect the catalytic efficiency of the reactions [11,12]. For instance, Zhang et al. found that hematite nanorods

with exposed {110} facets exhibited a better foreign ion confinement capacity ( $\text{Fe}^{2+}$ ) and a higher  $\text{H}_2\text{O}_2$  adsorption than hematite nanoplates with exposed {001} facets [13]. The result indicated that different morphologies of iron oxides could improve the catalytic activity in the Fenton-like reaction. Moreover, it was reported that the addition of transition metals (such as  $\text{Ti}^{4+}$ ,  $\text{Ce}^{4+}$ ,  $\text{V}^{4+}$ ,  $\text{Zr}^{4+}$ , etc.) into iron oxides enhanced the catalytic activity in the Fenton-like reaction [14–16]. According to the above literature, we proposed a brand-new idea, synthesis of shape-controlled metallic oxides, for improving the performance of heterogeneous Fenton-like catalysts. Unfortunately, the effect of the different morphologies of bimetallic oxide catalysts on the catalytic performance has not been investigated in detail, and the reaction mechanism was not clearly in the heterogeneous Fenton-like system.

Sulfamethazine (SMT), one of the pharmaceutically active compounds (PhACs), is widely used due to its use simplicity, high chemical stability, good antimicrobial activity, fast absorption, and low price [1]. So the SMT is often detected in the aquatic environment, and selected as a target pollutant. In the study, we prepared the shape-controlled  $\text{Fe}_2\text{O}_3$ – $\text{ZrO}_2$  catalysts, evaluated the  $\text{H}_2\text{O}_2$  adsorption/decomposition process to produce  $\cdot\text{OH}$  radicals, and investigated the effect of the morphology on the catalytic activity of the  $\text{Fe}_2\text{O}_3$ – $\text{ZrO}_2$  catalysts in the Fenton-like reaction for degrading SMT. Moreover, the reaction mechanism was proposed for the Fenton-like reaction over the shape-controlled  $\text{Fe}_2\text{O}_3$ – $\text{ZrO}_2$  catalysts.

## 2. Results and Discussions

### 2.1. Characterization of the Catalysts

#### 2.1.1. Scanning Electron Microscope (SEM) Analysis

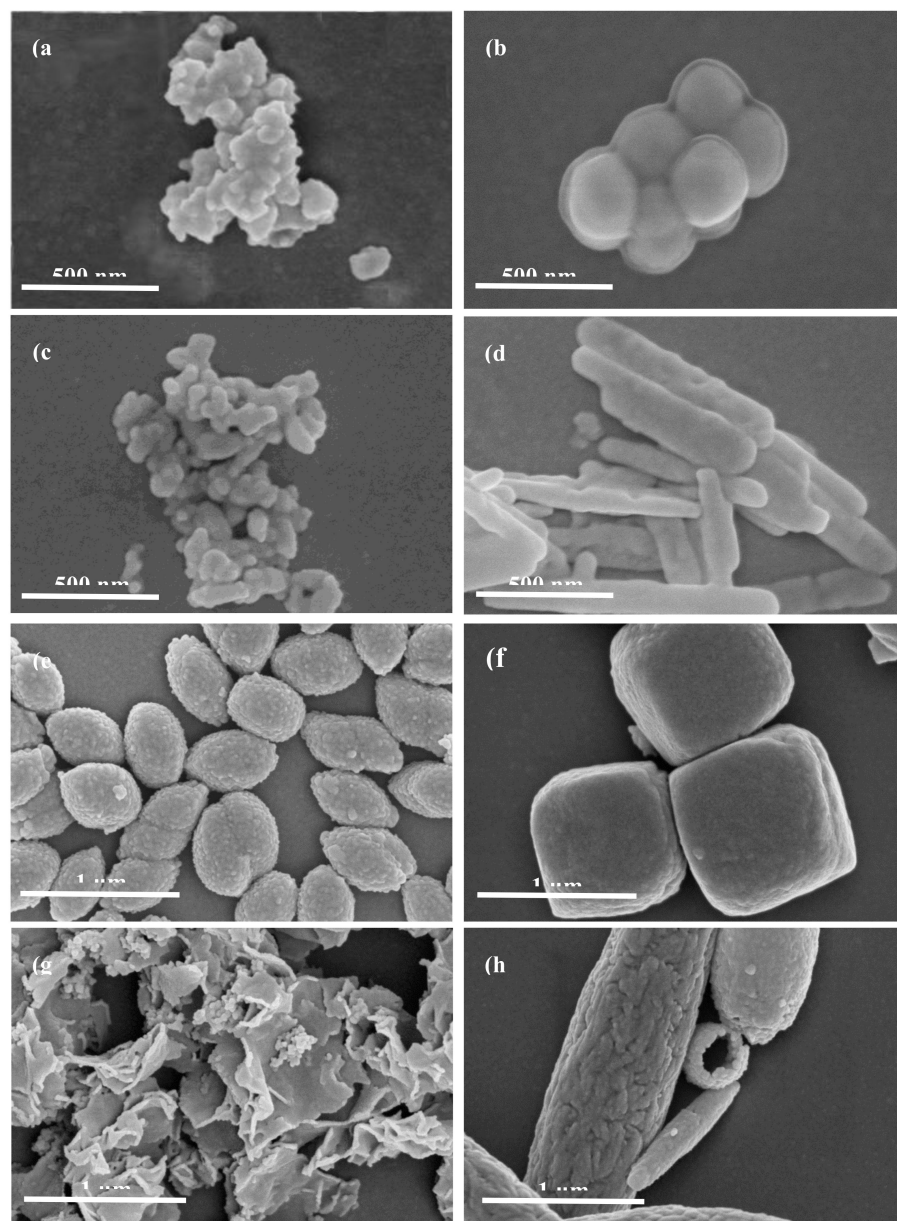
Figure 1 shows the morphologies of  $\text{Fe}_2\text{O}_3$  and  $\text{Fe}_2\text{O}_3$ – $\text{ZrO}_2$  catalysts in the SEM images. Pure  $\text{Fe}_2\text{O}_3$  with regular morphologies and sizes, involving nanoplates (HNPs), nanorods (HNRs), nanocubes (HNCs), and nanotubes (HNTs), was consistent with the literature [17,18]. Appropriate reagents (such as surfactant, additives, etc.) can affect the growth rate of various facets of  $\text{Fe}_2\text{O}_3$  in the growth process [11,19]. Moreover, the addition of metal ions effectively retained the aggregation of the catalysts, and led to the formation of a crystal particle with a smaller size [16]. The above results indicated that the smaller particle and similar morphology could be obtained with the Zr addition, in good agreement with our study (in Figure 1). For the  $\text{Fe}_2\text{O}_3$ – $\text{ZrO}_2$  catalysts with different morphologies, the nanoplates (HZNPs) exhibited an irregular plate-like structure, and the diameter decreased from ca. 214 nm to ca. 143 nm; the nanorods (HZNRs) became like short and thick sticks, and the length was obviously reduced from ca. 695 nm to ca. 217 nm; the nanocubes (HZNCs) evolved from cube to olive-shaped with a smaller size; the nanotubes (HZNTs) gradually lost the shape of nanotubes and formed a wrinkled sheet-like structure.

#### 2.1.2. X-ray Diffraction (XRD) and Brunauer–Emmett–Teller (BET) Analysis

For the shape-controlled  $\text{Fe}_2\text{O}_3$ – $\text{ZrO}_2$  catalysts, the XRD patterns revealed that diffraction peaks of  $\alpha$ - $\text{Fe}_2\text{O}_3$  with hexagonal crystal structure were observed, and weaker  $\text{ZrO}_2$  diffraction peaks were also observed (in Figure 2). Compared with  $\text{Fe}_2\text{O}_3$  (in Figure S1), the Zr addition weakened the intensity of  $\alpha$ - $\text{Fe}_2\text{O}_3$  peaks, suggesting that the Zr addition inhibited the  $\text{Fe}_2\text{O}_3$  agglomeration and reduced the  $\text{Fe}_2\text{O}_3$  crystallite size. According to the Scherrer's equation, the crystallite sizes of  $\alpha$ - $\text{Fe}_2\text{O}_3$  for HZNTs, HZNPs, HZNRs and HZNCs were 35, 47, 66, and 75 nm, respectively. As shown in Table 1, the surface areas for HZNTs, HZNPs, HZNRs, and HZNCs were 193, 107, 97, and  $66 \text{ m}^2/\text{g}$ , and obviously increased, compared with that of pure  $\text{Fe}_2\text{O}_3$  (in Table S1). The result was consistent with that of SEM of the  $\text{Fe}_2\text{O}_3$ – $\text{ZrO}_2$  catalysts.

### 2.1.3. X-ray Photoelectron Spectroscopy (XPS) Analysis

XPS analysis was used to characterize the chemical states of the shape-controlled  $\text{Fe}_2\text{O}_3$ - $\text{ZrO}_2$  catalysts. The Zr, O, and Fe peaks were observed at ca. 182, 530, and 711 eV, respectively (in Figure 3a). For pure  $\text{Fe}_2\text{O}_3$ , the Fe 2p<sub>3/2</sub> peak appeared at 710.6 eV and was attributed to  $\text{Fe}^{3+}$ -O. With the Zr addition, the binding energy of Fe 2p<sub>3/2</sub> shifted from 710.6 to 710.1 eV (in Figure 3b), indicating that the chemical state of Fe element changed in the  $\text{Fe}_2\text{O}_3$ - $\text{ZrO}_2$  catalysts. The Fe 2p<sub>3/2</sub> peaks were fitted into two peaks and assigned to  $\text{Fe}^{2+}$ -O (ca. 708.5 eV) and  $\text{Fe}^{3+}$ -O (ca. 710.6 eV) [20]. According to the fitting results, the different  $\text{Fe}^{2+}$  amounts for HNZPs, HNZRs, HNZCs, and HNZTs were 28, 18, 6, and 9 at. %, respectively. As iron oxides are used as catalysts in the Fenton-like reaction,  $\text{Fe}^{2+}$  favors the ·OH formation, and a high  $\text{Fe}^{2+}$  concentration is advantageous to improve the degradation of organic pollutants [16].

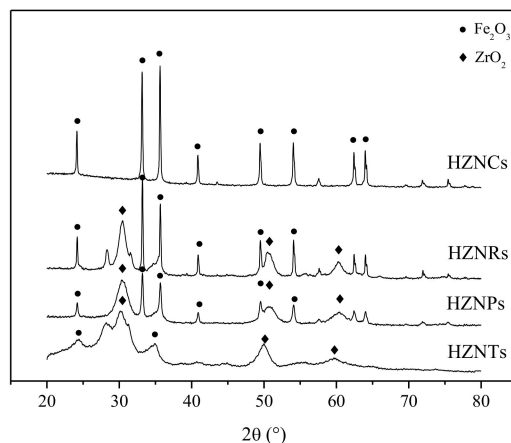
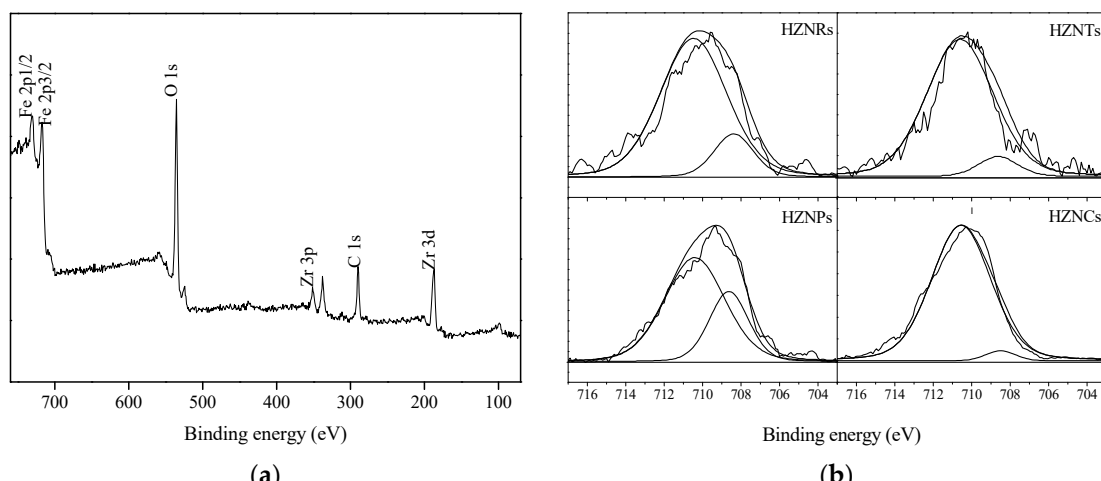


**Figure 1.** Scanning electron microscope (SEM) images on: (a)  $\text{Fe}_2\text{O}_3$ - $\text{ZrO}_2$  nanoplates (HZNPs), (b)  $\text{Fe}_2\text{O}_3$  nanoplates (HNPs), (c)  $\text{Fe}_2\text{O}_3$ - $\text{ZrO}_2$  nanorods (HZNRs), (d)  $\text{Fe}_2\text{O}_3$  nanorods (HNRs), (e)  $\text{Fe}_2\text{O}_3$ - $\text{ZrO}_2$  nanocubes (HZNCs), (f)  $\text{Fe}_2\text{O}_3$  nanoplates (HNCs), (g)  $\text{Fe}_2\text{O}_3$ - $\text{ZrO}_2$  nanotubes (HZNTs), (h)  $\text{Fe}_2\text{O}_3$  nanotubes (HNTs).

**Table 1.** Physicochemical properties of the shape-controlled  $\text{Fe}_2\text{O}_3$ – $\text{ZrO}_2$  catalysts.

Shape	$d_{\text{Fe}}$ [nm]	Surface Area [ $\text{m}^2/\text{g}$ ]	$\omega_{\text{Fe}}^{\text{a}}$ [wt. %]	SDIAs <sup>b</sup> [ $\text{Fe}/\text{nm}^2$ ]	$\tau_{\text{Fe}^{2+}}^{\text{c}}$ [at. %]	Density Site <sup>d</sup> [ $\text{Fe}^{2+}/\text{nm}^2$ ]
HZNPs	47	107	0.21	21.10	0.28	5.91
HZNRs	66	97	0.26	28.81	0.18	5.18
HZNCs	75	66	0.25	40.72	0.06	2.44
HZNTs	35	193	0.19	10.03	0.09	0.90

<sup>a</sup> The mass ratio of Fe on the catalysts surface; <sup>b</sup> SDIAs =  $\omega_{\text{Fe}} \times N_A / (\text{SSA} \times 56 \times 10^{18})$ ; <sup>c</sup> The atomic ratio of  $\text{Fe}^{2+}/(\text{Fe}^{2+} + \text{Fe}^{3+})$  on the catalysts surface; <sup>d</sup> Density Site = SDIAs ×  $\tau_{\text{Fe}^{2+}}$ .

**Figure 2.** X-ray diffraction (XRD) patterns of the shape-controlled  $\text{Fe}_2\text{O}_3$ – $\text{ZrO}_2$  catalysts.**Figure 3.** X-ray photoelectron spectroscopy (XPS) analysis (a) High-resolution spectrum of the HZNPs catalyst. (b) Fe 2p<sub>3/2</sub> XPS spectra of the shape-controlled  $\text{Fe}_2\text{O}_3$ – $\text{ZrO}_2$  catalysts.

## 2.2. The Activity of the $\text{Fe}_2\text{O}_3$ – $\text{ZrO}_2$ Catalysts

### 2.2.1. The Interaction of Hematite Facets with $\text{H}_2\text{O}_2$

The  $\text{H}_2\text{O}_2$  adsorption and activation on the catalyst surface are the important steps to produce ·OH radicals and degrade the pollutants in the heterogeneous Fenton-like reaction. High  $\text{H}_2\text{O}_2$  adsorption could favor the  $\text{H}_2\text{O}_2$  activation to produce ·OH radicals. Figure 4 shows the  $\text{H}_2\text{O}_2$  adsorption on the shape-controlled  $\text{Fe}_2\text{O}_3$ – $\text{ZrO}_2$  catalysts at pH 3.0 under 5 °C. The catalysts exhibited a rapid  $\text{H}_2\text{O}_2$  adsorption process, and then reached adsorption equilibrium. The order of the  $\text{H}_2\text{O}_2$  adsorption capacity was HZNPs > HZNRs > HZNCs > HZNTs, and the  $\text{H}_2\text{O}_2$  adsorption amounts on the catalysts were 45.6, 24.5, 16.3, and 14.3 mg/g<sub>cat</sub>, respectively. The normalized  $\text{H}_2\text{O}_2$  adsorption amount per

surface area of the  $\text{Fe}_2\text{O}_3$ – $\text{ZrO}_2$  catalysts was calculated, and is shown in Table 2. It was found that HZNPs showed the highest  $\text{H}_2\text{O}_2$  adsorption capacity ( $0.43 \text{ mg/m}^2$ ) which was ca. six times higher than that of HZNTs ( $0.07 \text{ mg/m}^2$ ).

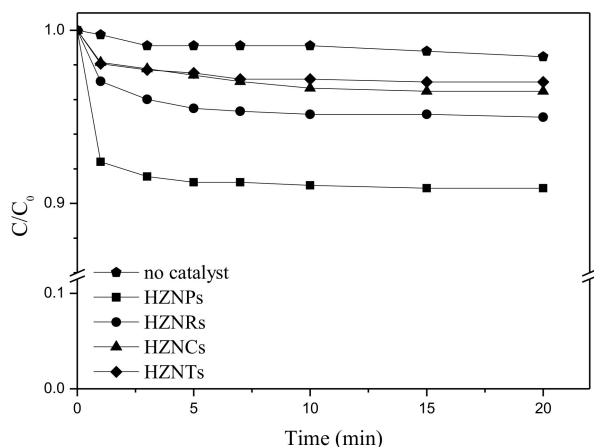


**Figure 4.** The  $\text{H}_2\text{O}_2$  absorption on the shape-controlled  $\text{Fe}_2\text{O}_3$ – $\text{ZrO}_2$  catalysts. ([Catalyst] = 0.5 g/L,  $[\text{H}_2\text{O}_2]_0 = 8 \text{ mmol/L}$ , pH = 3, T = 5 °C).

**Table 2.**  $\text{H}_2\text{O}_2$  absorption and decomposition properties of the shape-controlled  $\text{Fe}_2\text{O}_3$ – $\text{ZrO}_2$  catalysts.

Sample	$A_{\text{H}_2\text{O}_2}^{\text{a}}$ [mmol/L]	$A'_{\text{H}_2\text{O}_2}^{\text{b}}$ [mg/m <sup>2</sup> ]	$B_{\text{H}_2\text{O}_2}^{\text{c}}$ [%]	$k_{\text{H}_2\text{O}_2}^{\text{d}}$ [min <sup>-1</sup> ]	$k_{\text{H}_2\text{O}_2}/Q_{\text{H}_2\text{O}_2}$ [g/(mg·min)]
HZNPs	0.67	0.43	80.1	$6.70 \times 10^{-3}$	$1.47 \times 10^{-4}$
HZNRs	0.36	0.25	49.8	$3.00 \times 10^{-3}$	$1.23 \times 10^{-4}$
HZNCs	0.21	0.25	37.2	$2.00 \times 10^{-3}$	$1.23 \times 10^{-4}$
HZNTs	0.24	0.07	23.5	$1.20 \times 10^{-3}$	$8.40 \times 10^{-5}$

<sup>a</sup>  $\text{H}_2\text{O}_2$  maximum adsorption amount; <sup>b</sup> Adsorption amount of  $\text{H}_2\text{O}_2$  per unit area; <sup>c</sup>  $\text{H}_2\text{O}_2$  decomposition rate at 240 min; <sup>d</sup>  $\text{H}_2\text{O}_2$  decomposition rate constant.

The  $\text{H}_2\text{O}_2$  decomposition on the shape-controlled  $\text{Fe}_2\text{O}_3$ – $\text{ZrO}_2$  catalysts was evaluated at pH 3.0 and a temperature of 45 °C. As shown in Figure 5a, the  $\text{H}_2\text{O}_2$  decomposition rates of HZNPs, HZNRs, HZNCs, and HZNTs after 240 min reaction were 80%, 50%, 37%, and 24%, respectively. Moreover, the  $\text{H}_2\text{O}_2$  decomposition obeyed a pseudo-first kinetic equation (in Figure 5b). The apparent  $\text{H}_2\text{O}_2$  decomposition rate constants ( $k_{\text{H}_2\text{O}_2}$ ) were  $6.70 \times 10^{-3}$ ,  $3.00 \times 10^{-3}$ ,  $2.00 \times 10^{-3}$  and  $1.20 \times 10^{-3} \text{ min}^{-1}$ , and the order was HZNPs > HZNRs > HZNCs > HZNTs, respectively. To further investigate the  $\text{H}_2\text{O}_2$  decomposition efficiency on the  $\text{Fe}_2\text{O}_3$ – $\text{ZrO}_2$  catalysts, we normalized  $k_{\text{H}_2\text{O}_2}$  with its maximum adsorption capacity of  $\text{H}_2\text{O}_2$  ( $Q_{\text{H}_2\text{O}_2}$ ), and the result is shown in Table 2. It was observed that the  $k_{\text{H}_2\text{O}_2}/Q_{\text{H}_2\text{O}_2}$  of HZNPs with a lower surface area had the highest value which was ca. 1.8 times that of HZNTs with a higher surface area. The results indicated that: (1) the  $\text{H}_2\text{O}_2$  adsorption/decomposition process was related to the morphology, not to the surface area of the  $\text{Fe}_2\text{O}_3$ – $\text{ZrO}_2$  catalysts; (2) a higher adsorption/decomposition on the catalyst surface could be helpful to generate ·OH radicals in the Fenton-like reaction.

In the heterogeneous Fenton-like reaction, the ·OH radicals are known as the main active species for degrading organic compounds. To obtain insight on the ·OH radicals generated on the shape-controlled  $\text{Fe}_2\text{O}_3$ – $\text{ZrO}_2$  catalysts, a quantitative determination was carried out in the presence of  $\text{H}_2\text{O}_2$  at pH 3.0. For pure  $\text{Fe}_2\text{O}_3$ , there was almost no ·OH formation (not shown), despite a good  $\text{H}_2\text{O}_2$  adsorption obtained as shown in Figure S2. For the  $\text{Fe}_2\text{O}_3$ – $\text{ZrO}_2$  catalysts, the generated ·OH radicals were detected and the result was shown in Figure 6. The ·OH radicals rapidly increased in the initial 120 min reaction, and the concentration was ca. 241.8, 108.8, 72.9, and 35.9  $\mu\text{mol/L}$  for HZNPs, HZNRs, HZNCs, and HZNTs at 240 min, respectively. The HZNPs exhibited a higher  $\text{H}_2\text{O}_2$

decomposition rate and a greater ·OH concentration than the other catalysts. The normalized ·OH concentration per surface area of the catalysts in 240 min reaction was 4.52, 2.24, 2.20, and 0.37  $\mu\text{mol}/\text{m}^2$  for HZNPs, HZNRs, HZNCs, and HZNTs, respectively. The normalized ·OH amount of HZNPs was ca. 12 times that of HZNTs. The results further confirmed that the ·OH generation was independent of the specific surface area and was mainly affected by the morphologies of the  $\text{Fe}_2\text{O}_3$ – $\text{ZrO}_2$  catalysts. In addition, the free ·OH radicals generated were the main chemical state for total ·OH radicals in the Fenton-like reaction (in Figure S3). The shape-controlled  $\text{Fe}_2\text{O}_3$ – $\text{ZrO}_2$  catalysts favored the free ·OH formation when they reacted with  $\text{H}_2\text{O}_2$ . It was found that the free ·OH concentration for all catalysts was obviously higher than that of the SMT in the solution, indicating that the desorption of the generated ·OH radicals from the catalyst surface was not a limiting step for the SMT degradation in our experiments.

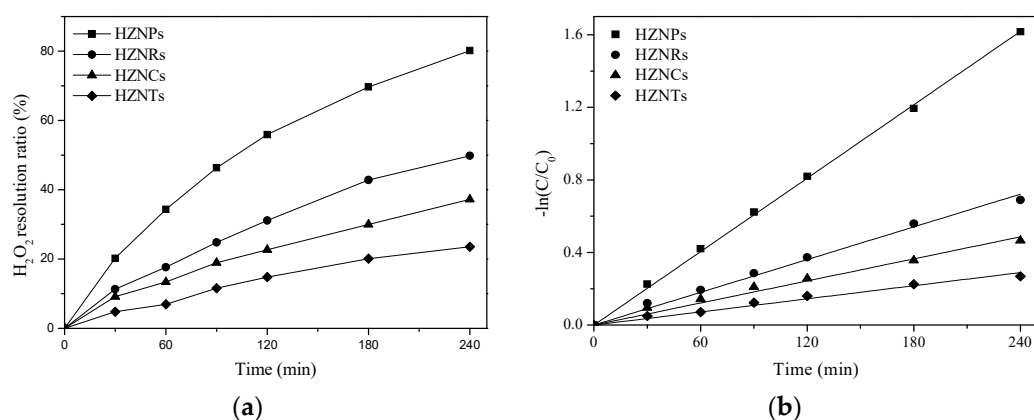


**Figure 5.** The  $\text{H}_2\text{O}_2$  decomposition and decomposition kinetics curves on the shape-controlled  $\text{Fe}_2\text{O}_3$ – $\text{ZrO}_2$  catalysts (a)  $\text{H}_2\text{O}_2$  decomposition curves; (b)  $\text{H}_2\text{O}_2$  decomposition kinetics curves ([Catalyst] = 0.5 g/L,  $[\text{H}_2\text{O}_2]_0$  = 8 mmol/L, pH = 3, T = 45 °C).

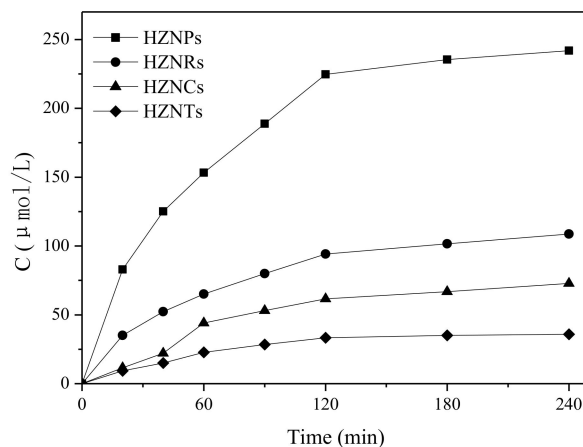


**Figure 6.** Quantitative determination of ·OH radicals generated by the shape-controlled  $\text{Fe}_2\text{O}_3$ – $\text{ZrO}_2$  catalysts in the presence of  $\text{H}_2\text{O}_2$ . ([Catalyst] = 0.5 g/L,  $[\text{H}_2\text{O}_2]_0$  = 8 mmol/L, pH = 3, T = 45 °C).

## 2.2.2. The Activity of the $\text{Fe}_2\text{O}_3$ – $\text{ZrO}_2$ Catalysts

The Fenton-like reaction degrading the SMT was conducted at pH 3.0 and with an initial SMT concentration of 10 mg/L over the shape-controlled  $\text{Fe}_2\text{O}_3$  and  $\text{Fe}_2\text{O}_3$ – $\text{ZrO}_2$  catalysts (see Figure S4 and Figure 7a). In the  $\text{H}_2\text{O}_2$  and  $\text{Fe}_2\text{O}_3$ / $\text{H}_2\text{O}_2$  systems, almost no SMT removal was obtained after 240 min, indicating that both systems were not active for removing SMT. In the heterogeneous  $\text{Fe}_2\text{O}_3$ – $\text{ZrO}_2$ / $\text{H}_2\text{O}_2$  system, the SMT removal significantly increased, while the SMT adsorption on the  $\text{Fe}_2\text{O}_3$ – $\text{ZrO}_2$  catalysts was negative (<5%). The result indicated that the shape-controlled  $\text{Fe}_2\text{O}_3$ – $\text{ZrO}_2$  catalysts exhibited good activity in the Fenton-like reaction of the SMT degradation. Moreover,

the activity order was as follows: HZNPs > HZNRs > HZNCs > HZNTs, and HZNPs exhibited the best catalytic activity, whose SMT removal reached 98% after 240 min.

As shown in Figure 7b, a pseudo-first kinetic equation was obtained in the Fenton-like reaction for the SMT degradation over the shape-controlled  $\text{Fe}_2\text{O}_3\text{-ZrO}_2$  catalysts. The apparent rate constants ( $k$ ) for HZNPs, HZNRs, HZNCs, and HZNTs were  $1.5 \times 10^{-2}$ ,  $6.8 \times 10^{-3}$ ,  $1.7 \times 10^{-3}$ , and  $9.3 \times 10^{-4} \text{ min}^{-1}$ , respectively. We normalized the rate constant ( $k$ ) with the surface area of the  $\text{Fe}_2\text{O}_3\text{-ZrO}_2$  catalysts. The value of HZNPs ( $1.4 \times 10^{-4} \text{ g} \times \text{min}^{-1} \times \text{m}^{-2}$ ) was the highest, which was ca. two times that of HZNRs ( $7.0 \times 10^{-5} \text{ g} \times \text{min}^{-1} \times \text{m}^{-2}$ ) and ca. 29 times that of HZNTs ( $4.8 \times 10^{-6} \text{ g} \times \text{min}^{-1} \times \text{m}^{-2}$ ). The results indicated that the activity of the shape-controlled  $\text{Fe}_2\text{O}_3\text{-ZrO}_2$  catalysts was closely related to the morphology, not the surface area of the catalysts.

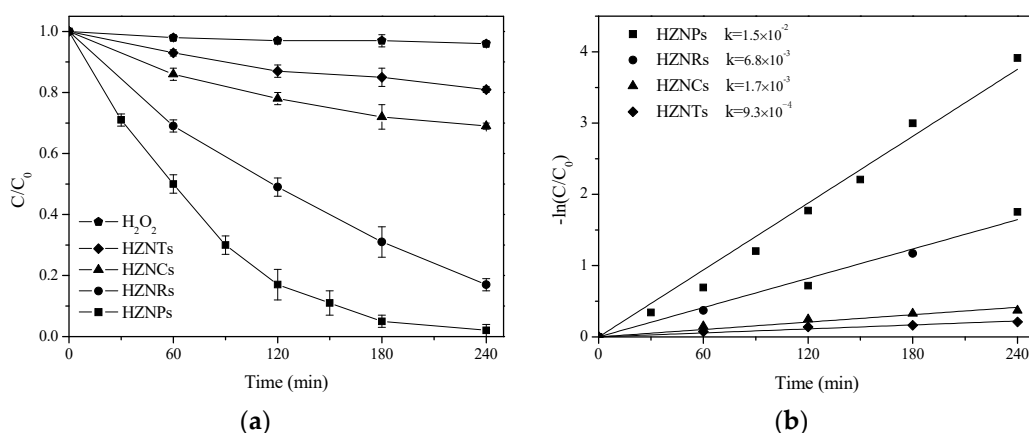


**Figure 7.** The sulfamethazine (SMT) removal efficiency and SMT removal kinetics curves in the Fenton-like reaction over the shape-controlled  $\text{Fe}_2\text{O}_3\text{-ZrO}_2$  catalysts (a) SMT removal efficiency. (b) SMT removal kinetics. ([Catalyst] = 0.5 g/L,  $[\text{H}_2\text{O}_2]_0$  = 8 mmol/L, pH = 3, T = 45 °C).

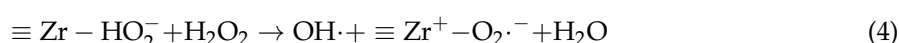
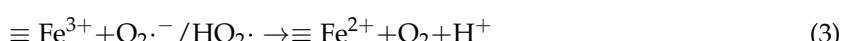
During the Fenton-like reaction, the Fe ion leaching was measured after 240 min, and a low concentration of Fe ion leaching was obtained (<0.2 mg/L). The results indicated that the  $\text{Fe}_2\text{O}_3\text{-ZrO}_2$  catalysts had good stability in the Fenton-like reaction for degrading SMT. The intermediates for the SMT degradation over HZNPs were detected by liquid chromatography–mass spectrometry (LC–MS). Several main intermediate products were obtained, including 4-amino-N-carbamimidoyl-benzenesulfonamide, 4,6-dimethyl-2-hydroxypyrimidine, sulfanilamide, aniline, and carboxylic acid, in good agreement with the literature [21].

### 2.3. Mechanism Analysis

In the heterogeneous Fenton-like reaction, the  $\text{H}_2\text{O}_2$  adsorption and the  $\text{H}_2\text{O}_2$  activation on the catalyst surface were the key steps limiting  $\cdot\text{OH}$  generation. In the literature [22], the adsorption of atoms, ions, and molecules on a catalyst surface is related to their morphologies, that is, the intrinsic crystal structure. For iron-based catalysts, the substance adsorption was both related to the exposed facets and the surface densities of the iron atoms (SDIAs) [13,17]. In our study, the order of the  $\text{H}_2\text{O}_2$  adsorption on pure  $\text{Fe}_2\text{O}_3$  was nanorods > nanoplates > nanocubes > nanotubes (see Figure S2), in agreement with the above result. With the Zr addition, the SDIAs decreased (in Table 1), and led to a decrease of  $\text{H}_2\text{O}_2$  adsorption on the  $\text{Fe}_2\text{O}_3\text{-ZrO}_2$  catalysts (in Figure 4). It was noticed that HZNPs and HZNRs showed an obvious change in  $\text{H}_2\text{O}_2$  adsorption. For  $\text{Fe}_2\text{O}_3$  nanoplates and nanorods, the main {001} and exposed {110} facets could adsorb the substances on the catalyst surface, and {110} facets had a higher reactivity than {001} facets in the adsorption process [13]. This suggested that  $\text{Fe}_2\text{O}_3$  nanorods exhibited a better adsorption capacity than  $\text{Fe}_2\text{O}_3$  nanoplates. Therefore, Zr ions, as foreign substances, could be easily confined on the  $\text{Fe}_2\text{O}_3$  nanorods, indicating that more Zr ions occupied the exposed facet of HZNRs. This result led to the decrease of the SDIAs on the HZNRs. HZNPs exhibited a better  $\text{H}_2\text{O}_2$  adsorption capacity than HZNRs.

Another key step limiting the ·OH generation, H<sub>2</sub>O<sub>2</sub> activation, had a close relationship with the Fe<sup>2+</sup> amount on the surface for the iron-based catalysts in the Fenton-like reaction [16]. The Zr addition obviously increased the surface area and induced the presence of Fe<sup>2+</sup> on the catalyst surface. Moreover, the Fe<sup>2+</sup> density site (Fe<sup>2+</sup>/nm<sup>2</sup>) of the Fe<sub>2</sub>O<sub>3</sub>–ZrO<sub>2</sub> catalysts (see Table 1) showed a closed relationship with the morphologies of the catalysts, rather than the surface areas. HZNPs with a low surface area had the highest Fe<sup>2+</sup> site density, suggesting that the morphology affected the Fe<sup>2+</sup> density sites on the surface of the Fe<sub>2</sub>O<sub>3</sub>–ZrO<sub>2</sub> catalysts.

In the heterogeneous Fenton-like system for degrading organic compounds, a radical chain reaction is commonly involved [2,5,6,16]. In our study, there were important reaction processes for ·OH radical generation, as follows. First, the H<sub>2</sub>O<sub>2</sub> adsorption was the first step for the H<sub>2</sub>O<sub>2</sub> activation to ·OH radicals on the catalyst surface. A higher H<sub>2</sub>O<sub>2</sub> adsorption was helpful to react with Fe<sup>2+</sup> on the catalysts and produce ·OH radicals. Second, the H<sub>2</sub>O<sub>2</sub> activation occurred according to the reaction between ≡Fe<sup>2+</sup> with the adsorbed H<sub>2</sub>O<sub>2</sub> by electron transfer (Equation (1)). The result suggested that the ·OH radical formation was attributed to the H<sub>2</sub>O<sub>2</sub> adsorption and Fe<sup>2+</sup> density sites on the Fe<sub>2</sub>O<sub>3</sub>–ZrO<sub>2</sub> catalysts. Then the ·OH radicals, adsorbed on the surface by weak chemical bonds, easily desorbed to the free ·OH radicals in the solution, and rapidly oxidized organic pollutants. In the Fenton-like reaction, ZrO<sub>2</sub> with an amorphous and small particle on the catalyst surface, enhanced the regeneration process of ≡Fe<sup>2+</sup> from ≡Fe<sup>3+</sup> in the presence of H<sub>2</sub>O<sub>2</sub> at a low pH value (Equations (2)–(4)) [16]. Therefore, in the Fenton-like reaction process over the Fe<sub>2</sub>O<sub>3</sub>–ZrO<sub>2</sub> catalysts, the higher H<sub>2</sub>O<sub>2</sub> adsorption and Fe<sup>2+</sup> density sites favored greater ·OH generation. The result suggested that HZNPs exhibited the best SMT removal, due to the highest H<sub>2</sub>O<sub>2</sub> adsorption and Fe<sup>2+</sup> density sites.



### 3. Materials and Methods

#### 3.1. Materials and Chemicals

In the experiments, chemical reagents without further purification were obtained from Aladdin Industrial Corporation in China. Methanol, acetic acid, and H<sub>2</sub>O<sub>2</sub> (30 wt.%) were purchased from the Sigma-Aldrich Company.

#### 3.2. Synthesis Methods

Fe<sub>2</sub>O<sub>3</sub> and Fe<sub>2</sub>O<sub>3</sub>–ZrO<sub>2</sub> catalysts were prepared by the hydrothermal method according to the literature [17,18]. The Fe to Zr atomic ratio was one.

##### 3.2.1. Preparation of Fe<sub>2</sub>O<sub>3</sub>–ZrO<sub>2</sub> and Fe<sub>2</sub>O<sub>3</sub> Nanoplates

Amounts of 1.092 g of FeCl<sub>3</sub> × 6H<sub>2</sub>O and 1.289 g of ZrOCl<sub>2</sub> × 8H<sub>2</sub>O were dissolved in ethanol (40 mL) with a trace addition of distilled water (2.8 mL) under vigorously stirring. Sodium acetate (3.2 g) was added under stirring for 1 h. Then, the mixture was sealed in a Teflon-lined stainless steel autoclave (Kenuo, Beijing, China, 100 mL) and maintained at 180 °C for 12 h. After natural cooling to room temperature, the resulting solid was washed with distilled water and ethanol several times to remove any impurities and dried at 100 °C overnight. Finally, the products were ground and calcined at 500 °C for 3 h under air to obtain HZNPs. Pure Fe<sub>2</sub>O<sub>3</sub> nanoplates (HNPs) were prepared in a similar way.

### 3.2.2. Preparation of Fe<sub>2</sub>O<sub>3</sub>–ZrO<sub>2</sub> and Fe<sub>2</sub>O<sub>3</sub> Nanorods

Amounts of 1.683 g of Fe(NO<sub>3</sub>)<sub>3</sub> × 9H<sub>2</sub>O and 1.788 g of Zr(NO<sub>3</sub>)<sub>4</sub> × 5H<sub>2</sub>O were dissolved in 45 mL of deionized water. After completely dissolving, NaOH solution (10 wt.%) was added dropwise to adjust the pH to 12 ± 0.1, and then the mixture was vigorously stirred for 30 min. The mixture was transferred into a Teflon-lined stainless steel autoclave (100 mL) and kept at 180 °C for 12 h. After washing and drying the precipitate as in the previous method, the solid was calcined at 500 °C for 3 h under air to obtain HZNPs. Pure Fe<sub>2</sub>O<sub>3</sub> nanorods (HNRs) were prepared in a similar way.

### 3.2.3. Preparation of Fe<sub>2</sub>O<sub>3</sub>–ZrO<sub>2</sub> and Fe<sub>2</sub>O<sub>3</sub> Nanocubes

Amounts of 0.811 g of FeCl<sub>3</sub> × 6H<sub>2</sub>O and 1.288 g of Zr(NO<sub>3</sub>)<sub>4</sub> × 5H<sub>2</sub>O were dissolved in 50 mL of cetyltrimonium bromide (CTAB) aqueous solution ( $C_{CTAB} = 0.04 \text{ mol/L}$ ) under vigorous stirring for 30 min, and then transferred into a Teflon-lined stainless steel autoclave (100 mL) and maintained at 120 °C for 12 h. After washing and drying the precipitate as in the previous method, the solid was calcined at 500 °C for 3 h under air to obtain HZNCs. Pure Fe<sub>2</sub>O<sub>3</sub> nanocubes (HNCs) were prepared in a similar way.

### 3.2.4. Preparation of Fe<sub>2</sub>O<sub>3</sub>–ZrO<sub>2</sub> and Fe<sub>2</sub>O<sub>3</sub> Nanotubes

Amounts of 1.081 g of FeCl<sub>3</sub> × 6H<sub>2</sub>O and 1.289 g of ZrOCl<sub>2</sub> × 8H<sub>2</sub>O were dissolved in 60 mL of NH<sub>4</sub>H<sub>2</sub>PO<sub>4</sub> solution ( $C_{NH_4H_2PO_4} = 0.04 \text{ mol/L}$ ). After stirring for 30 min, the mixture was transferred into a Teflon-lined stainless steel autoclave (100 mL) and kept at 220 °C for 12 h. After washing and drying as in the previous method, the solid was calcined at 500 °C for 3 h under air to obtain HZNTs. Pure Fe<sub>2</sub>O<sub>3</sub> nanotubes (HNTs) were prepared in a similar way.

## 3.3. Catalyst Characterization

The morphology of the catalysts was obtained by a Hitachi SU8010 field emission scanning electron microscope (FESEM) (Hitachi, Tokyo, Japan) using an accelerating voltage of 5 kV. The specific surface area of the catalysts was measured by N<sub>2</sub> adsorption at 77 K using an Autosorb iQ-MP system (Quantachrome Instruments, Boynton Beach, FL, USA). Before analysis, the sample was outgassed at 200 °C for 4 h. The X-ray diffraction (XRD) pattern of the catalysts was measured on a Bruker D8 Focus diffractometer (Bruker, Karlsruhe, Germany) using Cu K $\alpha$  radiation ( $\lambda = 0.15406 \text{ nm}$ ). X-ray photoelectron spectroscopy (XPS) analysis for the catalysts was performed on a PHI 5400 ESCA analyser with an Al K $\alpha$  X-ray source (PHI, Chanhassen, MN, USA) ( $h\nu = 1486.60 \text{ eV}$ ). The C1s peak ( $E_b = 284.60 \text{ eV}$ ) was used as a reference for the calibration of the binding energy.

## 3.4. H<sub>2</sub>O<sub>2</sub> and ·OH Concentration Measurement

Titanium oxalate spectrophotometry was used for detecting the H<sub>2</sub>O<sub>2</sub> concentration in the Fenton reaction. The concentration of hydroxyl radicals (·OH) was analyzed with a modified methanol probe molecule method [23]. Hydroxyl radicals reacted with methanol to form formaldehyde, and then the formaldehyde was determined by the 2,4-dinitrophenylhydrazine (DNPH) derivation method. The concentration of DNPH-formaldehyde derivative was measured by high-performance liquid chromatography (HPLC, Agilent 1260, Agilent, Santa Clara, CA, USA) with a C18 column at 400 nm.

## 3.5. Fenton Degradation Experiments

The experiments were performed in a 500 mL glass flask in the dark, equipped with a stirrer and a thermocouple. First, the initial pH of the SMT solution was adjusted to 3.0 ± 0.05 by adding 5 wt.% HCl, and then a catalyst and an SMT solution (10 mg/L, 250 mL) were loaded into the reactor with stirring. The reactor was heated to 45 °C, and then maintained for 30 min to achieve adsorption equilibrium on the catalyst. Secondly, H<sub>2</sub>O<sub>2</sub> was added into the reactor, and the point was defined as “zero” time of the Fenton-like reaction. Samples were periodically withdrawn from the reactor,

quenched with methanol, and then filtered through a 0.22  $\mu\text{m}$  filter. The SMT concentration was analyzed by HPLC. The mobile phase was composed of methanol and water ( $v/v = 60:40$ ). The flow rate was 1.0 mL/min and the detection wavelength was 254 nm.

#### 4. Conclusions

$\text{Fe}_2\text{O}_3$ – $\text{ZrO}_2$  catalysts with different morphologies were produced successfully by a hydrothermal method. The  $\text{H}_2\text{O}_2$  adsorption and the  $\text{Fe}^{2+}$  density sites had a combined effect on ·OH generation in the Fenton-like reaction over the  $\text{Fe}_2\text{O}_3$ – $\text{ZrO}_2$  catalysts. Moreover, the  $\text{H}_2\text{O}_2$  adsorption and the  $\text{Fe}^{2+}$  density sites depended on the morphology, rather than the specific surface area. The normalized  $\text{H}_2\text{O}_2$  adsorption capacity per surface area on the catalyst surface was 0.43 mg/m<sup>2</sup> for HZNPs, and ca. 1.68, 1.72 and 5.75 times that of HZNRs, HZNCs, and HZNTs, respectively. The  $\text{Fe}^{2+}$  density sites ( $\text{Fe}^{2+}/\text{nm}^2$ ) were 5.91, 5.18, 2.44, and 0.90 for HZNPs, HZNRs, HZNCs, and HZNTs, respectively. The normalized ·OH concentration per surface area of the catalysts was 4.52, 2.24, 2.20, and 0.37  $\mu\text{mol}/\text{m}^2$  for HZNPs, HZNRs, HZNCs, and HZNTs, respectively. HZNPs and HZNRs showed a more effective catalytic performance for degrading SMT at pH 3.0 in the Fenton-like reaction. This work indicated that the shape-controlled bimetallic oxides effectively improved the catalytic performance in the heterogeneous Fenton-like reaction.

**Supplementary Materials:** The following are available online at <http://www.mdpi.com/2073-4344/9/1/85/s1>, Figure S1: XRD patterns of the shape-controlled  $\text{Fe}_2\text{O}_3$  catalysts, Figure S2: The  $\text{H}_2\text{O}_2$  absorption with the shape-controlled  $\text{Fe}_2\text{O}_3$  catalysts, Figure S3: Free ·OH radicals and surface ·OH radicals generated by the shape-controlled  $\text{Fe}_2\text{O}_3$ – $\text{ZrO}_2$  catalysts in the presence of  $\text{H}_2\text{O}_2$ , Figure S4: The SMT removal in the Fenton-like reaction over the shape-controlled  $\text{Fe}_2\text{O}_3$  catalysts, Table S1: Detail information of the shape-controlled  $\text{Fe}_2\text{O}_3$  catalysts.

**Author Contributions:** Funding acquisition, P.G. and S.Y.; Investigation, Y.H., Y.S. and M.H.; Project administration, S.Y.; Validation, M.H.; Writing—review and editing, P.G.

**Funding:** This research received no external funding.

**Acknowledgments:** The work was supported by National Major Science and Technology Program for Water Pollution Control and Treatment (2017ZX07101-003) and Fundamental Research Funds for Central Universities (2018ZD08, 2018MS033).

**Conflicts of Interest:** The authors declare no conflict of interest.

#### References

- Wang, J.L.; Wang, S.Z. Removal of pharmaceuticals and personal care products (PPCPs) from wastewater: A review. *J. Environ. Manag.* **2016**, *182*, 620–640. [[CrossRef](#)] [[PubMed](#)]
- Anipsitakis, G.P.; Dionysiou, D.D. Radical generation by the interaction of transition metals with common oxidants. *Environ. Sci. Technol.* **2004**, *38*, 3705–3712. [[CrossRef](#)]
- Zhao, H.Y.; Qian, L.; Chen, Y.; Wang, Q.N.; Zhao, G.H. Selective catalytic two-electron  $\text{O}_2$  reduction for onsite efficient oxidation reaction in heterogeneous electro-Fenton process. *Chem. Eng. J.* **2018**, *332*, 486–496. [[CrossRef](#)]
- Xiao, J.D.; Xie, Y.B.; Cao, H.B.; Wang, Y.X.; Guo, Z.; Chen, Y. Towards effective design of active nanocarbon materials for integrating visible-light photocatalysis with ozonation. *Carbon* **2016**, *107*, 658–666. [[CrossRef](#)]
- Pereira, M.C.; Oliverira, L.C.A.; Murad, E. Iron oxide catalysts: Fenton and Fenton-like reactions—A review. *Clay Miner.* **2012**, *47*, 285–302. [[CrossRef](#)]
- Dhakshinamoorthy, A.; Navalon, S.; Alvaeo, M.; Garcia, H. Metal nanoparticles as heterogeneous Fenton catalysts. *ChemSusChem* **2012**, *5*, 46–64. [[CrossRef](#)] [[PubMed](#)]
- Suanon, F.; Sun, Q.; Li, M.Y.; Cai, X.; Zhang, Y.C.; Yan, Y.J.; Yu, C.P. Application of nanoscale zero valent iron and iron powder during sludge anaerobic digestion: Impact on methane yield and pharmaceutical and personal care products degradation. *J. Hazard. Mater.* **2017**, *321*, 47–53. [[CrossRef](#)] [[PubMed](#)]
- Wang, Y.B.; Zhao, H.Y.; Zhao, G.H. Iron-copper bimetallic nanoparticles embedded within ordered mesoporous carbon as effective and stable heterogeneous Fenton catalyst for the degradation of organic contaminants. *Appl. Catal. B* **2015**, *164*, 396–406. [[CrossRef](#)]

9. Sun, J.Q.; Chen, Y.L.; Chen, J.G. Morphology effect of one-dimensional iron oxide nanocatalysts on Fischer-Tropsch synthesis. *Catal. Sci. Technol.* **2016**, *6*, 7505–7511. [[CrossRef](#)]
10. Wang, B.H.; Sun, J.Q.; Abbas, M.; Liu, Y.T.; Kong, F.H.; Xiao, H.C.; Chen, J.G. A Novel Hydrothermal Approach for the Synthesis of Flower-Like  $\text{Fe}_2\text{O}_3/\text{Fe}$  Foam Nanocrystals and Their Superior Performance in Fisher-Tropsch Synthesis. *Catal. Lett.* **2017**, *147*, 1153–1161. [[CrossRef](#)]
11. Su, M.H.; He, C.; Shih, K. Facile synthesis of morphology and size-controlled  $\alpha\text{-Fe}_2\text{O}_3$  and  $\text{Fe}_3\text{O}_4$  nano-and microstructures by hydrothermal/solvothermal process: The roles of reaction medium and urea dose. *Ceram. Int.* **2016**, *42*, 14793–14804. [[CrossRef](#)]
12. Hou, L.W.; Zhang, Q.H.; Jérôme, F.; Duprez, D.; Zhang, H.; Royer, S. Shape-controlled nanostructured magnetite-type materials as highly efficient Fenton catalysts. *Appl. Catal. B* **2014**, *144*, 739–749. [[CrossRef](#)]
13. Huang, X.P.; Hou, X.J.; Zhao, J.C.; Zhang, L.Z. Hematite facet confined ferrous ions as high efficient Fenton catalysts to degrade organic contaminants by lowering  $\text{H}_2\text{O}_2$  decomposition energetic span. *Appl. Catal. B* **2016**, *181*, 127–137. [[CrossRef](#)]
14. Wan, Z.; Wang, J.L. Degradation of sulfamethazine using  $\text{Fe}_3\text{O}_4\text{-Mn}_3\text{O}_4$ /reduced graphene oxide hybrid as Fenton-like catalyst. *J. Hazard. Mater.* **2017**, *324*, 653–664. [[CrossRef](#)] [[PubMed](#)]
15. Liang, X.L.; He, Z.S.; Zhong, Y.H.; Tan, W.; He, H.P.; Yuan, P.; Zhu, J.X.; Zhang, J. The effect of transition metal substitution on the catalytic activity of magnetite in heterogeneous Fenton reaction: In interfacial view. *Coll. Surf. A* **2013**, *435*, 28–35. [[CrossRef](#)]
16. Gao, P.; Song, Y.; Hao, M.J.; Zhu, A.N.; Yang, H.W.; Yang, S.X. An effective and magnetic  $\text{Fe}_2\text{O}_3\text{-ZrO}_2$  catalyst for phenol degradation under neutral pH in the heterogeneous Fenton-like reaction. *Sep. Purif. Technol.* **2018**, *201*, 238–243. [[CrossRef](#)]
17. Gao, Q.X.; Wang, X.F.; Di, J.L.; Wu, X.C.; Tao, Y.R. Enhanced catalytic activity of  $\alpha\text{-Fe}_2\text{O}_3$  nanorods enclosed with {110} and {001} planes for methane combustion and CO oxidation. *Catal. Sci. Technol.* **2011**, *1*, 574–577. [[CrossRef](#)]
18. Chen, L.Q.; Yang, X.F.; Chen, J.; Wu, J.H.; Zhan, H.Q.; Liang, C.L.; Wu, M.M. Continuous shape- and spectroscopy-tuning of hematite nanocrystals. *Inorg. Chem.* **2010**, *49*, 8411–8420. [[CrossRef](#)] [[PubMed](#)]
19. Wu, W.; Yang, S.L.; Pan, J.; Sun, L.L.; Zhou, J.; Dai, Z.G.; Xiao, X.H.; Zhang, H.B.; Jiang, C.Z. Metal ion-mediated synthesis and shape-dependent magnetic properties of single-crystalline  $\alpha\text{-Fe}_2\text{O}_3$  nanoparticles. *CrystEngComm* **2014**, *16*, 5566–5572. [[CrossRef](#)]
20. Scheffe, J.R.; Francés, A.; King, D.M.; Liang, X.H.; Branch, B.A.; Cavanagh, A.S.; George, S.M.; Weimer, A.W. Atomic layer deposition of iron(III) oxide on zirconia nanoparticles in a fluidized bed reactor using ferrocene and oxygen. *Thin Solid Films* **2009**, *517*, 1874–1879. [[CrossRef](#)]
21. Wan, Z.; Wang, J.L. Degradation of sulfamethazine antibiotics using  $\text{Fe}_3\text{O}_4\text{-Mn}_3\text{O}_4$  nanocomposite as a Fenton-like catalyst. *J. Chem. Technol. Biotechnol.* **2017**, *92*, 874–883. [[CrossRef](#)]
22. Wu, C.Z.; Yin, P.; Zhu, X.; OuYang, C.Z.; Xie, Y. Synthesis of hematite ( $\alpha\text{-Fe}_2\text{O}_3$ ) nanorods: Diameter-size and shape effects on their applications in magnetism, lithium ion battery, and gas sensors. *J. Phys. Chem. B* **2006**, *110*, 17806–17812. [[CrossRef](#)] [[PubMed](#)]
23. Goldstein, S.; Aschengrau, D.; Diamant, Y.; Rabani, J. Photolysis of aqueous  $\text{H}_2\text{O}_2$ : Quantum yield and applications for polychromatic UV actinometry in photoreactors. *Environ. Sci. Technol.* **2007**, *41*, 7486–7490. [[CrossRef](#)] [[PubMed](#)]



© 2019 by the authors. Licensee MDPI, Basel, Switzerland. This article is an open access article distributed under the terms and conditions of the Creative Commons Attribution (CC BY) license (<http://creativecommons.org/licenses/by/4.0/>).